CFD INJECTION SIMULATION OF DIETHYL ETHER INTO A DIESEL INTAKE MANIFOLD

Sergiu STROE, Rodica NICULESCU, Adrian CLENCI
University of Pitesti, Str. Tîrgu din Vale nr.1, Pitesti, 110040, Romania

Abstract: *Computational fluid dynamics modeling has come a long way since its entrance into engineering industry over 20 years ago. Increases in the power of computer hardware, together with decreasing of hardware costs, have allowed CFD software tools to be developed to offer the high-tech capabilities we see today.*

A three-dimensional unsteady turbulent compressible FLUENT solver was used in the present study to investigate the injection of diethyl ether into the intake manifold of a direct injection diesel engine, as a method to improve the cold starting characteristics.

The complete engine flow field, the inlet jet, pressure variation in the intake manifold and ports, and formation of blend in the intake ports, is also clearly shown.

Keywords: Diesel fuel spray, droplet breakup, evaporation, CFD, cold start.

INTRODUCTION

When a cold engine is started, an overreach supply of fuel must be supplied to assure enough fuel vapors to create a combustible gas mixture. When the walls of the intake system and cylinders are cold, a much smaller percentage of the fuel will vaporize than in normal steady-state operation. The fuel is also cold and does not flow as readily. The engine turns very slowly, being driven only by the starting motor, and a greater amount of the compressive heating during compression is lost by heat transfer to the cold walls. This is made worse by the cold viscous lubricating oil that resists motion and slows the starting speed even more. All of these factors contribute to the need for a very rich air-fuel ratio when starting a cold engine.

That said this paper we propose the following solution to improve cold start of diesel engines. The method involves injecting a combustible substance (ether) inside the engine intake manifold to improve the quality of the cold. This is a special starting fluid for aiding engine startup in extremely cold temperatures. Even when everything is very cold, a small percentage of fuel vaporizes and a combustible air and vapor mixture can be obtained. This mixture is ignited, and after only a few cycles of combustion, the engine begins to heat up. Within a few seconds it starts to operate in a more normal mode, but it can take many minutes before fully warmed steady-state operation is reached. Once the engine starts to warm, all of the excess fuel that was originally input vaporizes and a short period of overreach operation is experienced. During this period, there is a large excess of HC and CO emissions in the exhaust. To compound this problem, the catalytic converter is also cold at startup and does not remove these excess emissions.

Substances like diethyl ether with very high vapor pressures evaporate more readily than gasoline and give a richer air-fuel vapor mixture for initiating combustion. These fluids generally are obtained in pressurized containers and are sprayed into the engine air intake before starting.

DRIVING MATHEMATICAL MODELS AND COMPUTER SIMULATION

Many mathematical models have been developed to help understand, correlate, and analyze the operation of engine cycles. These include combustion models, models of physical properties, and models of flow into, through, and out of the cylinders. Even though models often cannot represent processes and properties to the finest detail, they are a powerful tool in the understanding and development of engines and engine cycles. With the use of models and computers in the design of new engines and components, great savings are made in time and cost. Historically, new design was a costly, time-consuming practice of trial and error, requiring new-part construction and testing for each change. Now engine changes and new designs are first developed on the computer using the many models which exist. Often, only after a component is optimized on the computer is a part actually constructed and tested.

Generally, only minor modifications must then be made to the actual component. Models range from simple and easy to use, to very complex and requiring major computer usage. In general, the more useful and accurate models are quite complex. Models to be used in engine analysis are developed using empirical relationships and approximations, and often treat cycles as quasi-steady-state processes. Normal fluid flow equations are often used. Some models will treat the entire flow through the engine as one unit, some will divide the engine into sections, and some will subdivide each section (e.g., divide the combustion chamber into several zones-burned and unburned, boundary layer near the wall, etc.). Most models deal only with one cylinder, which eliminates any interaction from multi- cylinders that can occur, mainly in the exhaust system.

This section describes the mathematical model for turbulent particle dispersion and vaporization assuming that the particles are sufficiently dispersed so that particle–particle interaction is negligible.

The particle phase is described using a Lagrangian approach while an Eulerian frame is used to describe the effects of both inter-phase slip and turbulence on particle motion using random-sampling techniques (Monte Carlo). It is also assumed that the mean flow is steady and the material properties of the phases are constant.

When vaporizing droplets are involved in the simulations, two-way coupling must be accounted for since the phase change modifies the characteristics of the fluid phase. The vapor produced by the droplets is a mass source for the fluid; moreover the vaporization process generates modifications in the momentum and energy balances between both phases. Fluid-phase equations then contain many extra source terms. It is assumed that the vapor production does not significantly modify the fluid-phase density.

The method to solve the continuous phase is based on the solution of the conservation equations for momentum and mass. Turbulence is modeled with the ‘‘k - ω’’ turbulence model of Launder and Spalding [4], which is widely and thoroughly tested, and was found to predict reasonably well the mean flow [5]. In order to reduce the numerical errors to an acceptable level, the higher-order QUICK scheme of Leonard [6] is used to evaluate the convection terms. A similar method has been used for three-dimensional [5] or axisymmetric flows [7–9] and only the main features are summarized here.

The governing equations (continuity, momentum, turbulent kinetic energy, dissipation, enthalpy, and vapor mass fraction) constitute a set of coupled partial differential equations that can be reduced to a single convective–diffusive conservation equation of the form:

$$\frac{\partial(\rho U_i \phi)}{\partial X_i} = \frac{\partial}{\partial X_i}\left[\Gamma_\phi \frac{\partial \phi}{\partial X_i}\right] + S_\phi \, , \tag{1}$$

where $\Gamma\phi$ is the effective diffusion coefficient for quantity ϕ. The term on the left-hand side is the convection term, whilst the first and the second terms on the right-hand side are the diffusion term and the source term, respectively.

The source term $S\phi$ as divided into two parts, which yields the following expression:

$$S_\phi = S_{\phi g} + S_{\phi p} \, , \tag{2}$$

where $S\phi$ specifies the source term of the gas and $S\phi p$ specifies the source term of the particle.

The source terms of the gas phase, $S\phi g$ and the effective diffusion coefficient $\Gamma\phi$, are summarized in Table 1 for different depended variables. *G* is the usual turbulence energy production term defined as

$$G = \mu_t \left[\frac{\partial \overline{U_i}}{\partial X_j} + \frac{\partial \overline{U_j}}{\partial X_i}\right] \frac{\partial \overline{U_i}}{\partial X_j} \, , \tag{3}$$

and

$$\mu_t = C_\mu \rho \frac{k^2}{\varepsilon}, \tag{4}$$

Table 1
Terms in the general form of the differential equation

ϕ	$S\phi g$	$\overline{S\phi p}$	$\Gamma\phi$
1	-	$\overline{S\rho, p}$	-
U_i	$-\frac{\partial}{\partial X_i}\left(P+\frac{2}{3}k\right)-\frac{\partial}{\partial X_j}\frac{2}{3}\mu_t\frac{\partial \overline{U_j}}{\partial X_i}+\rho g_i$	$\overline{SU_i, p}$	$\mu+\mu_t$
T	0	$\overline{S_T, p}$	$\frac{\mu}{\Pr}+\frac{\mu}{\Pr_t}$
Yp	0	$\overline{S_Y, p}$	$\frac{\mu}{Sc}+\frac{\mu}{Sc_t}$
k	G-ρε	$\overline{S_k, p}$	$\mu+\frac{\mu_t}{\sigma_k}$
ε	$C_{\varepsilon 1}\frac{\varepsilon}{k}G-C_{\varepsilon 2}\rho\varepsilon$	$\overline{S_\varepsilon, p}$	$\mu+\frac{\mu_t}{\sigma_\varepsilon}$

Table 2
Turbulence model constants

Cμ	Cε1	Cε2	σ_k	σ_ε	Cε3	Pr_t	Sc_t	Pr	Sc
0.09	1.44	1.92	1.0	1.3	1.1	0.6	0.85	$\mu Cp/k_g$	μ/ρD

The turbulence model constants that are used are those indicated by Launder and Spalding [4] that have given good results for a large number of flows, and are summarized in Table 2. To describe the vaporization phenomena the model of Barata [18], which is based on the Abrazom and Sirignano [2] approach, is used in the present study. The convection effects are taken into account by introducing empirical correlation laws.

The main assumptions of the models are: spherical symmetry; quasi-steady gas film around the droplet; uniform physical properties of the surrounding fluid; uniform pressure around the droplet; and liquid/vapor thermal equilibrium on the droplet surface. The effect of the convective transport caused by the droplet motion relative to the gas was accounted for by the so-called ‘‘film theory’’, which results in modified correlations for the Nusselt and Sherwood numbers. For rapid evaporation (i.e. boiling effects) additional corrections were applied. The infinite droplet conductivity model was used to describe the liquid side heat transfer taking into account droplet heat-up. Hence, two differential equations for the temporal changes of droplet size and temperature have to be solved:

$$\frac{dD_p}{dt} = -\frac{2\dot{m}}{\pi\rho_F D_p^2}, \tag{5}$$

$$\frac{dT_p}{dt} = -\frac{6Q_L}{\pi\rho_F C_{pF} D_p^3}, \tag{6}$$

Under the assumption of steady-state conditions in the gas film and assuming a spherical control surface around the droplet, the total mass flow through this surface will be equal to the evaporation rate $\dot{m}$:

$$\dot{m} = \pi \overline{\rho_g D_g} D_p Sh \ln(1+B_M), \tag{7}$$

and

$$\dot{m} = \pi \frac{\overline{K_{vap}}}{Cp_{vap}} D_p Nu \ln(1 + B_T), \tag{8}$$

The quantity $\overline{\rho_g D_g}$ can be replaced with *Kvap/Cpvap* , assuming a Lewis number of unity, and the heat penetrating into the droplet can be expressed by

$$Q_L = \dot{m}\left(\frac{\overline{C_{vap}}(T_\infty - T_S)}{B_M} - L(T_S)\right), \tag{9}$$

For any given value of surface temperature, the vapor pressure is readily estimated from the Clausius–Claperyon equation as

$$P_{Fs} = \exp\left(a - \frac{b}{T_S - 43}\right), \tag{10}$$

where a and b are constants of the fuel. The latent heat of vaporization is given by Watson [11] as

$$L(T_S) = L_{tbn}\left(\frac{T_{cr} - T_S}{T_{cr} - T_{bn}}\right)^{-0.38}, \tag{11}$$

Eqs. (7) and (8) for $\dot{m}$ are similar to the expressions for the droplet vaporization rate predicted by the classical model, with the values of the non-dimensional parameters Nu_0 and Sh_0 in the classical formulas substituted by Nu* and Sh*, respectively. Where are expressed as

$$Sh_0 = 2 + (Sh_0 - 2)/F_M, \tag{12}$$

$$Nu_0 = 2 + (Nu_0 - 2)/F_T, \tag{13}$$

The parameters *Nu** and *Sh** are the ‘‘modified’’ Nusselt and Sherwood numbers, and tend to Nu_0 and Sh_0, respectively, as F_T and F_M tend to the unity. In the case of an isothermal surface and constant physical properties of the fluid, the problem has a selfsimilar solution and the correction factors F_M and F_T do not depend on the local Reynolds number. It was found that the values F_M and F_T are practically insensitive to the Schmidt and Prandtl numbers and the wedge angle variations, and can be approximated as

$$F_M = F(B_M),\; F_T = F(B_T), \tag{14}$$

where $F(B)$ is given by

$$F(B) = (1 + B)^{0.7}\frac{\ln(1 + B)}{B}. \tag{15}$$

Nu_0 and Sh_0 are evaluated by the Frossling correlations

$$Nu_0 = 2 + 0.552\,\mathrm{Re}^{1/2}\,\mathrm{Pr}^{1/3}, \tag{16}$$

$$Sh_0 = 2 + 0.552\,\mathrm{Re}^{1/2}\,Sc^{1/3}. \tag{17}$$

The evaporation rate m with convection is

$$\dot{m} = \pi \overline{\rho_g D_g} D_p \ln(1 + B_M)\left(2 + \frac{0.552\,\mathrm{Re}^{1/2}\,Sc^{1/3}}{F_M}\right) \tag{18}$$

and

$$\dot{m} = \pi \frac{\overline{K_{vap}}}{Cp_{vap}} D_p \ln(1 + B_T)\left(2 + \frac{0.552\,\mathrm{Re}^{1/2}\,\mathrm{Pr}^{1/3}}{F_T}\right). \tag{19}$$

The Schmidt number and the Prandtl number are equal assuming a Lewis number of unity. Eq. (18) has the advantage that it applies under all conditions, including the transient state of droplet heat-up, whereas Eq. (19) can only be used for steady-state evaporation.

Finally the evaporation rate $\dot{m}$ is

$$\dot{m} = \pi \frac{\overline{K_{vap}}}{Cp_{vap}} D_p \ln(1+B_M) \left(2 + \frac{0.552 \, \mathrm{Re}^{1/2} \, \mathrm{Pr}^{1/3}}{F_M} \right) \tag{20}$$

and the equations for the temporal changes of droplet size and temperature are:

$$\frac{dDp}{dt} = -\frac{4K_{vap} \ln(1+B_M)}{Cp_{vap} \rho_F D_p} \left(1 + \frac{0.276 \, \mathrm{Re}^{1/2} \, \mathrm{Pr}^{1/3}}{F_M} \right) \tag{21}$$

$$\frac{dTp}{dt} = -\frac{12K_g \ln(1+B_M)}{Cv_{vap} \rho_F D_p^2 Cp_F} \left(1 + \frac{0.276 \, \mathrm{Re}^{1/2} \, \mathrm{Pr}^{1/3}}{F_M} \right) \times \left(\frac{C_{vap}(T_\infty - T_S)}{B_M} - L(T_S) \right) \tag{22}$$

Of the air/vapor mixture in the boundary layer near the droplet surface according to Hubbard et al. [12], the best results are obtained using the one-third role of Sparrow and Gregg [13], where average properties are evaluated at the following reference temperature and composition:

$$T_r = T_S + \frac{T_\infty - T_S}{3}, \tag{23}$$

$$Y_{Fr} = Y_{Fs} + \frac{Y_{F\infty} - Y_{Fs}}{3}. \tag{24}$$

For example, the reference specific heat at constant pressure is obtained as a

$$Cp_{vap} = Y_{Ar}(Cp_{Ar} \text{ at } \mathrm{T_r}) + \mathrm{Y_{Fr}}\,(\mathrm{C_{pF}} \text{ at } \mathrm{T_r}) \tag{25}$$

The dispersed phase was treated using the Lagrangian reference frame. Particle trajectories were obtained by solving the particle momentum equation through the Eulerian fluid velocity field, for a sufficiently high number of trajectories to provide a representative statistics.

The equations used to calculate the position and velocity of each particle were obtained considering the usual simplification for dilute particle-laden flows [7,14]. Static pressure gradients are small, particles can be assumed spherical and particle collisions can be neglected. Since $\frac{\rho_p}{\rho_f} > 200$, the effects of Basset, virtual mass, Magnus, Saffman and buoyancy forces are negligible [3, 9]. In dilute flows of engineering interest, the steady-state drag term is the most important force acting on the particle. Under these conditions the simplified particle momentum equation is

$$\frac{\partial u_{p;i}}{\partial t} = \frac{1}{\tau_p}(u_{f;i} - u_{p;i}) + g_i. \tag{26}$$

The mathematical expression for the relaxation time, τ_p, is

$$\tau_p = \frac{24 \rho_p D_p^2}{18 \mu_f C_D \mathrm{Re}_P}, \tag{27}$$

where Re_P is the particle Reynolds number

$$\mathrm{Re}_P = \frac{\rho_f \left| \overrightarrow{V_P} - \overrightarrow{V_f} \right| D_p}{\mu_f}. \tag{28}$$

Note that the physical properties of ρ_f and μ_f should be evaluated at the reference temperature T_r and are

$$\mu_f = Y_{Ar}(\mu_A \text{ at } \mathrm{T_r}) + \mathrm{Y_{Fr}}\,(\mu_F \text{ at } \mathrm{T_r}) \tag{29}$$

$$\rho_{vap} = \left(\frac{Y_{Ar}}{\rho_A} + \frac{Y_{Fr}}{\rho_F} \right)^{-1} \tag{30}$$

and C_D is the drag coefficient [14], which was determined from the experimental data compiled by Schlichting [15]. The particle momentum equation can be analytically solved over small time steps, Δt, and the particle trajectory is given by

$$u_{p;i}^{NEW} = u_{f;i} + \left(u_{p;i}^{OLD} - u_{f;i}\right)e^{-\Delta t/\tau_p} + g_i \tau_p \left[1 - e^{-\Delta t/\tau_p}\right] \tag{31}$$

$$x_{p;i}^{NEW} = x_{p;i}^{OLD} + \frac{\Delta t}{2}\left(u_{p;i}^{NEW} + u_{p;i}^{OLD}\right) \tag{32}$$

The critical issues are to determine the instantaneous fluid velocity and the evaluation of the time, Δt, of interaction of a particle with a particular eddy. The time step is obviously the eddy-particle interaction time, which is the minimum of the eddy lifetime, τ_{FL}, and the eddy transit time, t_c. The eddy lifetime is estimated assuming that the characteristic size of an eddy is the dissipation length scale in isotropic flow:

$$l_e = B\frac{k^{3/2}}{\varepsilon} \approx C_\mu^{3/4}\frac{k^{3/2}}{\varepsilon}, \tag{33}$$

$$\tau_{FL} = A\frac{k}{\varepsilon} \approx 0.2\frac{k}{\varepsilon}, \tag{34}$$

where A and B are two dependent constants [14]. The transit time, t_c, is the minimum time a particle would take to cross an eddy with characteristic dimension, l_e, and is given by

$$t_c = \frac{l_e}{\left|\overrightarrow{v_d}\right|}, \tag{35}$$

where $\overrightarrow{v_d}$ is the relative velocity between the particle and the fluid (drift velocity).

A different expression for the transit time is also recommended in the literature [14, 16, and 17], and was used in the present work:

$$t_c = -\tau_p \ln\left(1 - \frac{l_e}{\tau_p\left|u_{f;i} - u_{p;i}\right|}\right), \tag{36}$$

where the drift velocity is also estimated at the beginning of a new iteration.

This equation has no solution when le> $\tau_p\left|u_{f;i} - u_{p;i}\right|$, that is, when the linearized stopping distance of the particle is smaller than the eddy size. In such a case, the particle can be assumed to be trapped by the eddy, and the interaction time will be the eddy lifetime. The instantaneous velocity at the start of a particle–eddy interaction is obtained by random sampling from an isotropic Gaussian pdf having standard deviations of $\sqrt{\frac{2}{3}k}$ and zero mean values.

CALCULUS MODEL AND REQUIREMENTS OF THE LIMIT CONDITIONS

Geometry and mesh generation

The geometry and meshing of the intake manifold was created using CATIA V5R19 and ANSA software's, and are represented in Figure1.

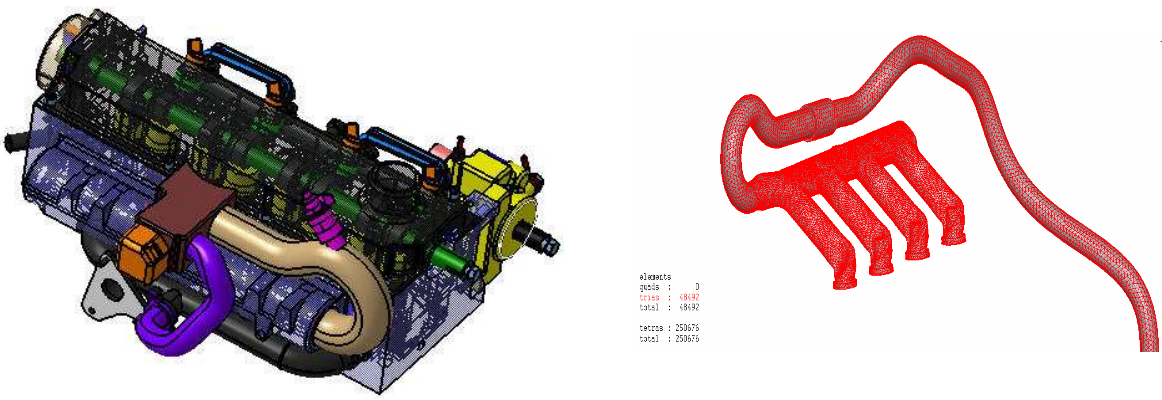

Figure 1. Geometry model and mesh generation

Boundary conditions

Regarding the boundary conditions, simulation is done considering the mean temperature 250 K (-23^{0}C), inlet pressure in the intake manifold is atmospheric, and for each drum part was considered a depression in the intake valve of 0.96 bar.

Injection of combustible substance begins practically from the moment t = 0 seconds and lasts for the entire period of numerical simulation. In the table below are shown the conditions to limit the air intake manifold and fuel injection substance.

Table1. Boundary conditions of the model.

Intake manifold pressure [Pa]	101325
Valve inlet pressure [Pa]	97272
Intake valve diameter [mm]	36
Mass flow rate [kg/s]	0.002
Ambient temperature [^{0}K]	250
Injection velocity [m/s]	32

Setting the injector position

As shown in the figure below have been taken into account three arbitrary position of the location area of the injector on the manifold to establish the correct position of the injector.

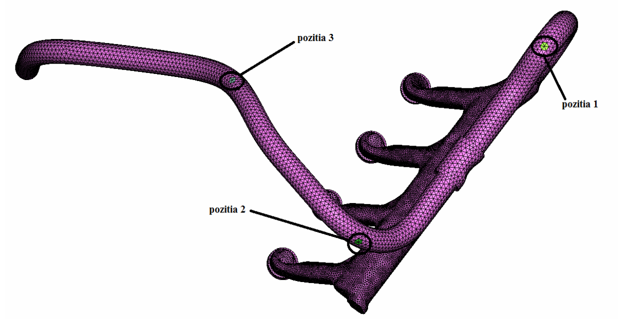

Figure 2. Injector positions on the intake manifold.

RESULTS AND CONCLUSIONS

Considering the case of cold start simulation was performed by injecting a combustible substance for 1 second for all four cylinders which it follows that for each drum part during the simulation is 0.25 seconds, after which the data post processing was performed. That means for each cylinder was performed three analyses.

In case of cylinder 1 compared with the three-position of the injector the results are shown in figures bellow:

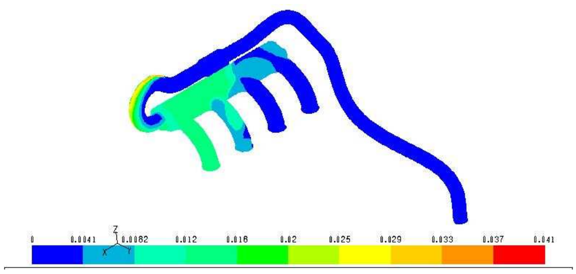

Figure 3 ***Mass fraction of combustible substance admitted to the cylinder 1 for the position of injector.***

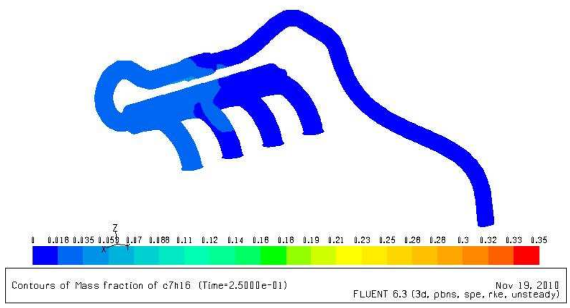

Figure 4 ***Mass fraction of combustible substance admitted in the cylinder 1 for the second position of injector.***

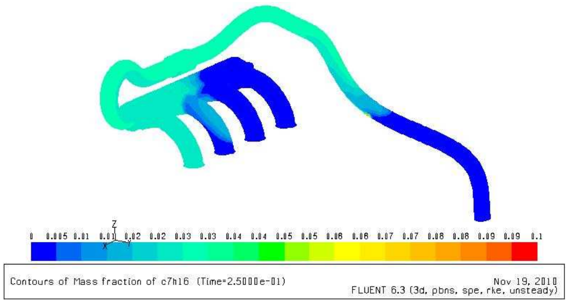

Figure 5 ***Mass fraction of combustible substance admitted to the cylinder 1 for the third position of injector.***

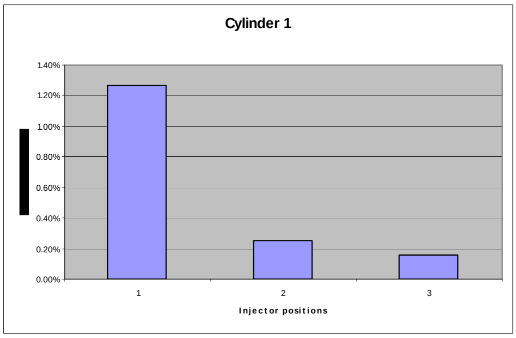

Figure 6 Mass fraction compared results: cylinder 1 vs. positions

So for that cylinder the results are [1.27%] (the percent of mass fraction which is admitted in cylinder) obtained for the first position of the injector.

For the second cylinder the results are shown in figures below:

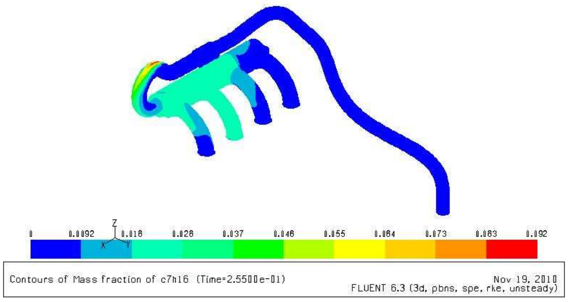

Figure 7 ***Mass fraction of combustible substance admitted to the cylinder 2 for the position of injector.***

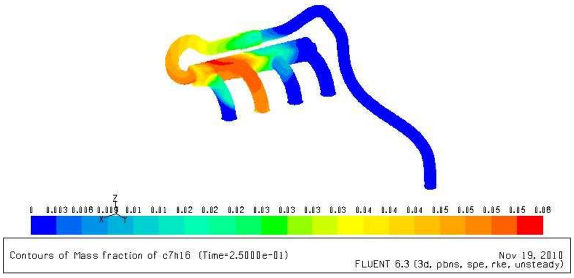

Figure 8 ***Mass fraction of combustible substance admitted in the cylinder 2 for the second position of injector.***

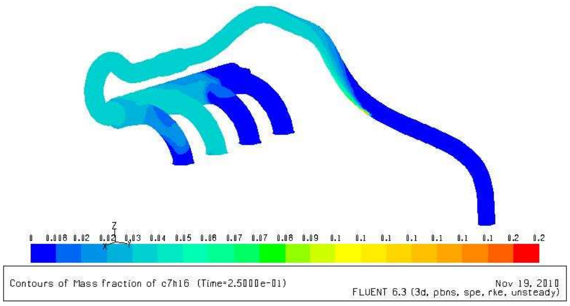

Figure 9 ***Mass fraction of combustible substance admitted to the cylinder 2 for the third position of injector.***

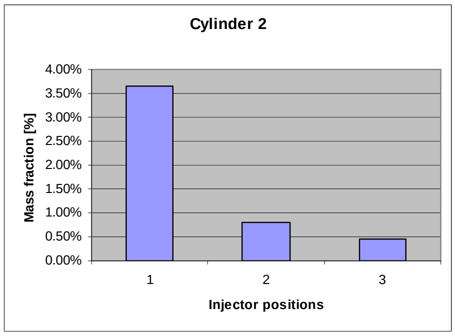

Figure 10 Mass fraction compared results: cylinder 2 vs. positions

Comparing the results with those obtained for the first cylinder can be seen that in this cylinder, the percentage of mass fraction entering the cylinder is double. The maximum percentage 3.64 [%] is done in case of the first position.

For the third cylinder were obtained the following results:

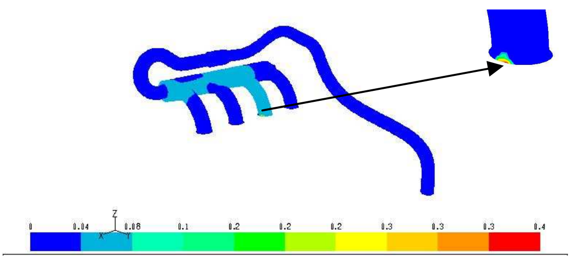

Figure 11 ***Mass fraction of combustible substance admitted to the cylinder 3 for the position of injector.***

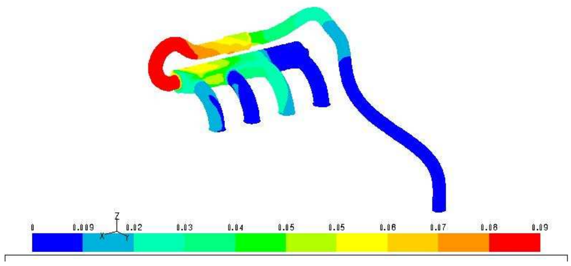

Figure 12 ***Mass fraction of combustible substance admitted in the cylinder 3 for the second position of injector.***

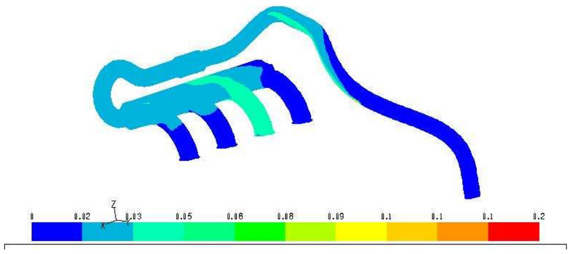

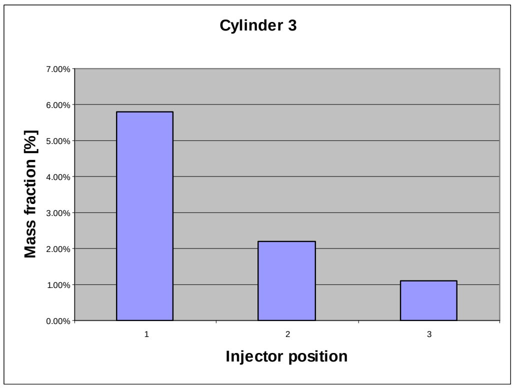

Figure 13 ***Mass fraction of combustible substance admitted to the cylinder 3 for the third position of injector.***

Figure 14 ***Mass fraction compared results: cylinder 3 vs. positions***

For the third cylinder is observed that in case of simulation of the first position of injector (figure 11.), the phenomenon of evaporation of mass fractions appears and their quantity is calculated as 0.15 grams.

We found the same injector position from which we obtain the best results for mass fractions like 5.8 [%].

Regarding the simulation results for the fourth cylinder is shown as if the other cylinders in the next figure.

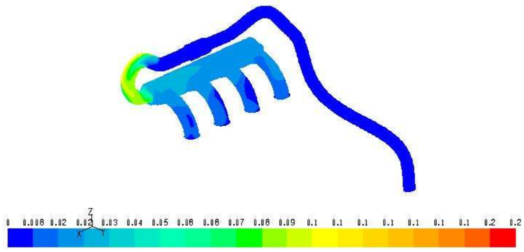

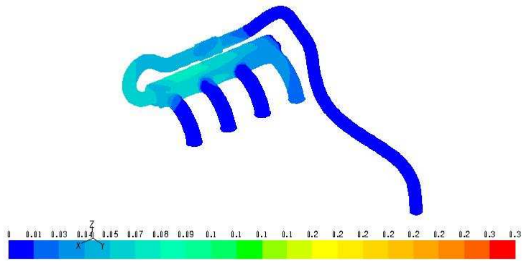

Figure 15 ***Mass fraction of combustible substance admitted to the cylinder 4 for the position of injector.***

Figure 16 ***Mass fraction of combustible substance admitted in the cylinder 4 for the second position of injector.***

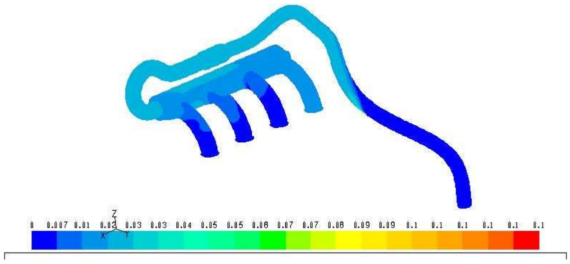

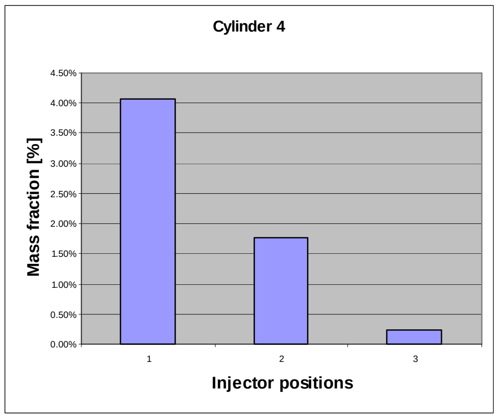

Figure 17 ***Mass fraction of combustible substance admitted to the cylinder 4 for the third position of injector.***

Figure 18 Mass fraction compared results: cylinder 4 vs. positions

Again, notice that the first position in which combustible substance is injected is most favorable in terms of percentage of mass fraction which is entering in the cylinder. The maximum value is 4.08 [%].

The results were summarized in the table and diagram below to be more easily compared between the four-cylinder and three positions of which are injected.

Table 2. Percent of mass fraction. Cylinders vs. injector positions

		Cylinders			
		1	2	3	4
	1	1.27%	3.64%	5.80%	4.08%
Injector positions	2	0.25%	0.81%	2.20%	1.76%
	3	0.16%	0.46%	1.09%	0.24%

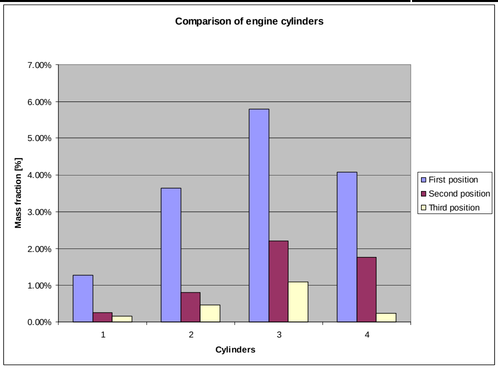

Figure 19. Injector positions on the intake manifold.

According to the numerical results and analysis mentioned above, some conclusions are drawn as follows:

This study was done in order to find optimal solution mounting additional intake manifold injector. As is apparent from the numerical simulations showed that the injector should be placed in position as a combustible substance injected into this position through a shorter distance and thus the mass fractions of mixture reach combustible substance in excess of engine cylinders. Note that if additional injector mounts on the other two positions arbitrarily chosen mass fraction ratios reaching very much lower in the engine cylinders. The only cylinder that the combustible substance comes in the vapor mixture is cylinder number 3, namely 0.15 g. This subject is also to be developed within the frame of the research project, which is financially supported by the Romanian Council for Scientific Research in the Higher Education (CNCSIS).

ACKNOWLEDGEMENTS

The authors would like to express their gratitude to the Romanian Council for Scientific Research in the Higher Education (CNCSIS) for their financial grant, thus making this study possible.

REFERENCES

[1] J. Barata, *Modelling of biofuel droplets dispersion and evaporation* Aerospace Sciences Department, Universidade Beira Interior, Rua Marques A ´ vila e Bolama, 6201-001 Covilha˜, Portugal Received 7 January 2007; accepted 29 April 2007 Available online 21 June 2007

[2] Abramzon B, Sirignano WA. *Droplet vaporization model for spray combustion calculations. Int J Heat Mass Transfer 1989;12(9):1605–48.*

[3] Arcoumanis C, Whitelaw DS, Whitelaw JS. *Gasoline injection against surfaces and films. Atomization Sprays 1997;7:437–56.*

[4] Launder BE, Spalding DB. *The numerical computation of turbulent flows. Computational Methods Appl Mech Eng 1974;3:269–89.*

[5] Barata JMM. *Jets in ground effect with a crossflow. AIAA J 1998;36(9):1737–40.*

[6] Leonard BP. *A stable and accurate convective modeling procedure based on quadratic upstream interpolation. Comput Methods ApplMech Eng 1979;19(1):59–98.*

[7] Shuen JS, Solomon ASP, Zhang QF, Faeth GM. *Structure of a particle-laden jets: measurements and predictions. AIAA J 1985;23(3):396–404.*

[8] Lilley DG. *Primitive pressure – velocity code for the computation of strongly swirling flows. AIAA J 1976;14(6):749–56.*
[9] Lockwood FC, Naguib AS. *The prediction of the fluctuations in the properties of free, round jet, turbulent, diffusion flames. Combustion Flame 1975;24:109–24.*
[10] Barata JMM. *On the modelling of droplet transport, dispersion and evaporation in turbulent flows. In: International congress on combustion engines (PTNSS KONGRES 2005), Bilezko-Biala, Szczyrk, Poland, 25–28 September 2005.*
[11] Watson KM. *Prediction of critical temperatures and heats of vaporization. Ind Eng Chem 1931;23(4):360–4.*
[12] Hubbard GL, Denny VE, Mills AF. Int J *Heat Mass Transfer 1973;16:1003–8.*
[13] Saparrow EM, Gregg JL. *Trans ASME 1958;80:879–86.*
[14] Shirolkar JS, Coimbra CFM, Queiroz McQuay M. *Fundamentals aspects of modeling turbulent particle dispersion in dilute flows. Program Energy Combustion Science 1996;22:363–99.*
[15] Schlichting H. *In: Gersten K, editor. Boundary layer theory. Springer, Berlin, Heidelberg: GmbH & Co.; 1999.*
[16] Gosman AD, Ioannides E. *Aspects of computer simulation of liquid fuelled combustors. In: AIAA 19th aerospace sciences meeting, AIAA paper no. 81-0323, St. Louis, MO, 1981.*
[17] Ranz WE, Marshall Jr WR. *Evaporation from drops. Chemical Engineering Program 1952;48:141–73.*
[18] Lefebvre AH. *Atomization and sprays. New York: Hemisphere Pub. Co.; 1989.*